Thermodynamic Properties of 1-Butyl-3-methylimidazolium Hexafluorophosphate in the Ideal Gas State†

Yauheni U. Paulechka, Gennady J. Kabo,* Andrey V. Blokhin, and Oleg A. Vydrov

Belarusian State University, Chemical Faculty, Leningradskaya 14, Minsk 220050, Belarus

Joseph W. Magee and Michael Frenkel

Physical and Chemical Properties Division, National Institute of Standards and Technology, 325 Broadway, Boulder, Colorado 80305-3328

Thermodynamic properties of an ionic liquid 1-butyl-3-methylimidazolium hexafluorophosphate ([C_4mim][PF_6]) in the ideal gas state were calculated from molecular and spectral data. Because quantum chemical calculations demonstrated that K_{dis} for [C_4mim][PF_6] did not exceed 10^{-11} at temperatures below 1000 K, the gas was assumed to consist of ion pairs. The product of the principal moments of inertia was found to be 16.49×10^{-132} kg^3·m^6. The frequencies of normal vibrations were obtained from the experimental and calculated spectra. Rotation of CH_3—N═ was assumed to be free. The parameters for all alkyl tops were taken to be close to those in alkanes. The parameters for Bu- and PF_6 were calculated ab initio. The calculated thermodynamic functions of the ideal gas ($S°$, C_p, and $-(G° - H°(0))/T$) were (657.4, 297.0, and 480.3) J·K^{-1}·mol^{-1}, respectively, at 298 K and were (843.1, 424.4, and 252.8) J·K^{-1}·mol^{-1}, respectively, at 500 K. Experiments were performed to better characterize the thermal stability and vapor pressure P_{sat} of this substance. DSC experiments were carried out in a temperature range from (303 to 523) K and suggest that the substance starts to decompose at temperatures greater than 473 K. Knudsen effusion experiments were attempted to measure P_{sat} for [C_4mim][PF_6] in the temperature range (433 to 522) K, but no reproducible values of P_{sat} were obtained. By combining a published value of the cohesive energy density, measured heat capacities, and thermodynamic properties in the ideal gas state, thermodynamic properties of vaporization ($\Delta^g_{liq}C_p$, $\Delta_{vap}S$, $\Delta_{vap}H$) and vapor pressure (P_{sat}) were calculated. At room temperature, the calculated P_{sat} was found to be 10^{-10} Pa, a value that is much smaller than the lower detection limit for effusion measurements.

Introduction

Ionic liquids (ILs) that melt near ambient temperatures have shown potential as new solvents and extracting agents. They can make extraction more effective and selective and have the potential to be continuously recycled in a process. A knowledge of the physical and chemical properties of ILs is needed to accelerate and optimize their use, which could result in a lower impact on the environment and enhanced development of waste-free technologies. Ideal gas thermodynamic functions are essential to this effort. To assess technically and ecologically reasonable conditions for ILs (T, P, etc.) and to provide for their recycling in processes, it is also essential to know their limits of thermal stability and saturated vapor pressure P_{sat}. Since ILs were assumed a priori to have extremely low P_{sat} at ambient temperatures, we anticipated experimental challenges to measuring reliable values.

In this work, thermodynamic properties of an ionic liquid, 1-butyl-3-methylimidazolium hexafluorophosphate ([C_4mim][PF_6]), in the ideal gas state were calculated from molecular and spectra data. This substance was selected because it is typical of the dialkylimidazolium class of air and water stable ionic liquids and was commercially available with a high purity. For this purpose, a series of calculations has been performed to obtain the geometry of ion pairs, parameters of internal rotation, and harmonic vibrational frequencies. A calorimetric experiment was used to explore the limits of thermal stability. We also attempted to determine P_{sat} for [C_4mim][PF_6] by the Knudsen technique, a method that is characterized by effusion through a membrane orifice into high vacuum. We have also computed P_{sat} with the ideal gas thermodynamic properties for [C_4mim][PF_6], measured heat capacities, and a published value of the cohesive energy density.

Experimental Section

Treatment of Samples and DSC Measurements. (We use trade names to specify the experimental procedure and materials adequately and do not imply endorsement by the National Institute of Standards and Technology. Similar products by other manufacturers may work as well or better.) Initially, a small sample of [C_4mim][PF_6], from Covalent Associates, Inc., with a mass of 21.1 mg was investigated with a Mettler FP99 differential scanning calorimeter in the range (300 to 670) K. The experimental results for a scan rate of 10 K·min^{-1} are shown in Figure 1. An endothermic effect of around 0.3 J·g^{-1} was observed in the temperature range (400 to 420) K. The original commercially supplied sample was an electrochemical grade one that was certified by the manufacturer to contain an H_2O composition of <20 ppm. Nevertheless, it appears that a sufficient quantity of H_2O was present to promote

† This contribution will be part of a special print edition containing papers presented at the Workshop on Ionic Liquids at the 17th IUPAC Conference on Chemical Thermodynamics, Rostock, Germany, July 28 to August 2, 2002.

* Corresponding author. Phone/Fax: +375-17-2203916. E-mail: kabo@bsu.by.

10.1021/je025591i CCC: $25.00
Published on Web 11/01/2002

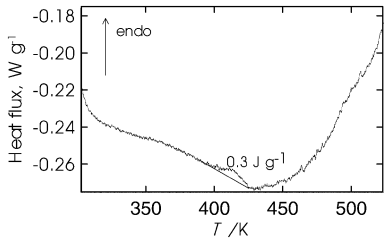

Figure 1. DSC heat flux curve for the [C_4mim][PF_6] sample.

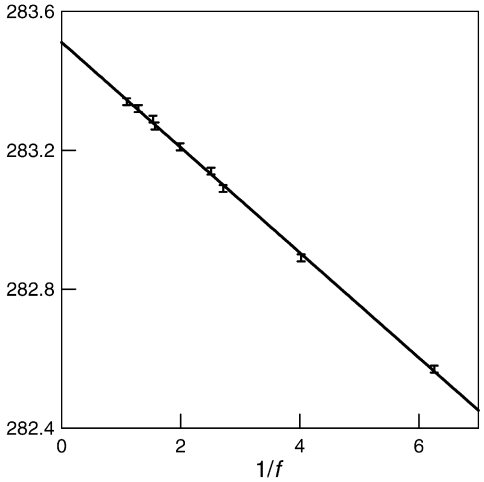

Figure 2. Determination of the purity of [C_4mim][PF_6] by a fractional melting technique with an adiabatic calorimeter; f is the fraction of the sample that had melted; $\Delta_{fus}H°(283.51\ K) = 19.60\ kJ·mol^{-1}$.

hydrolysis of the [PF_6] ion. This reaction should be avoided in the laboratory, since it would evolve HF. Thus, additional drying of our sample would be needed before further experimentation. Furthermore, the DSC curve shows another endothermic effect, above 450 K, increasing sharply with temperature at $T > 473$ K. This endothermic effect was probably due to decomposition. Thus, the DSC scans indicate that [C_4mim][PF_6] is thermally stable at $T < 473$ K, but decomposition had started above this temperature.

After the initial DSC, the following sample preparation technique was used to remove volatile impurities such as H_2O and air that might participate in reactions at $T > 400$ K. First, the commercial [C_4mim][PF_6] samples were vacuum pumped for 3 h at 293 K. The measured mass loss was 0.08 mass %. Additional vacuum pumping for 2 h resulted in no further reduction in mass. Then, the pumped sample was charged into a Knudsen cell and vacuum pumped for more than 10 h at 430 K. The measured mass losses averaged 0.08 mass %. The final sample purity of this sample was determined by a fractional-melting procedure in a low-temperature adiabatic calorimeter to be 99.56 mol %, as shown in Figure 2. The DSC curve for the sample prepared as described above was essentially the same as that for the initial commercial sample prior to degassing.

Knudsen Study of [C_4mim][PF_6]. Both the apparatus for the integral Knudsen effusion method and the technique of measurement have been described in detail.[1] A degassed sample with a mass of 0.3 g was charged into a stainless steel cell with an internal diameter of 1.00 cm and a volume of 0.8 cm^3. The cell was sealed with a Teflon ring. Two membranes with orifice diameters of (0.8254 and 3.00) mm and thicknesses of (0.050 and 2.20) mm, respectively, were used in the experiments at a residual pressure of 10^{-3} Pa.

The temperature was controlled within ±0.02 K in a liquid thermostatic bath. The temperature of the cell was measured with a platinum resistance thermometer. The mass of the cell with the sample was determined with a balance with an uncertainty of $\pm 2 \times 10^{-5}$ g. The elapsed time was measured from the moment when the residual pressure in the system dropped to 10^{-2} Pa until gaseous helium was supplied to the surroundings at the end of the effusion experiment. An experimentally determined correction of 54 s, for mass loss during unsteady conditions before the residual pressure had reached 10^{-2} Pa, was added to the elapsed effusion time. For this instrument, the working range of pressures is (0.01 to 100) Pa.

Table 1. Measured Temperature T, Time τ, Orifice Area S, Membrane Thickness l, and Mass Loss Δm for Effusion Experiments[a] (Uncertainties: $\delta\tau = \pm 2$ s; $\delta T = \pm 0.02$ K; $\delta\Delta m = 2 \times 10^{-5}$ g)

expt	T / K	τ / s	$\Delta m \times 10^6$ / kg	$(\Delta m)/(\tau S) \times 10^4$ / kg·s^{-1}·m^{-2}	comments on liquid
	Membrane No. 1, $S = (5.351 \pm 0.001) \times 10^{-7}$ m^2, $l = 0.050 \times 10^{-3}$ m				
1	477.96	36 054	0.27	0.140	
2	477.69	18 054	0.18	0.186	colorless
3	493.06	18 059	2.72	2.81	
4	492.73	10 854	0.83	1.43	yellow
5	522.66	7 344	3.08	7.84	
6	521.90	7 254	3.17	8.17	
7	522.40	18 054	9.09	9.41	dark yellow
	Membrane No. 2, $S = (7.069 \pm 0.047) \times 10^{-6}$ m^2, $l = 2.2 \times 10^{-3}$ m				
8	433.30	9 054	0.19	3.0×10^{-2}	
9	463.04	14 574	0.37	3.6×10^{-2}	colorless
	Open Cell, $S = (78.54 \pm 0.16) \times 10^{-6}$ m^2				
10	473.15	18 000	0.70	5.0×10^{-3}	colorless
	Membrane No. 2, $S = (7.069 \pm 0.047) \times 10^{-6}$ m^2, $l = 2.2 \times 10^{-3}$ m				
11	473.18	14 754	0.47	4.5×10^{-2}	
12	483.35	18 054	1.05	8.2×10^{-2}	
13	478.01	18 054	0.95	7.4×10^{-2}	dark yellow

[a] One sample was used in experiments 1−7; a second sample was used in experiments 8−13.

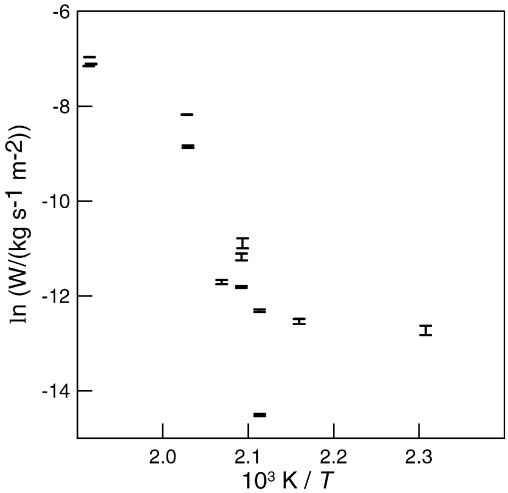

Figure 3. Temperature dependence of the specific mass loss rate from a Knudsen effusion cell.

The effusion results are given in Table 1. To compare them, we plotted the logarithm of the specific mass loss rate, ln W, against reciprocal temperature in Figure 3,

$$W = \frac{\Delta m}{\tau S} \tag{1}$$

where Δm is the mass loss during an elapsed time τ, and

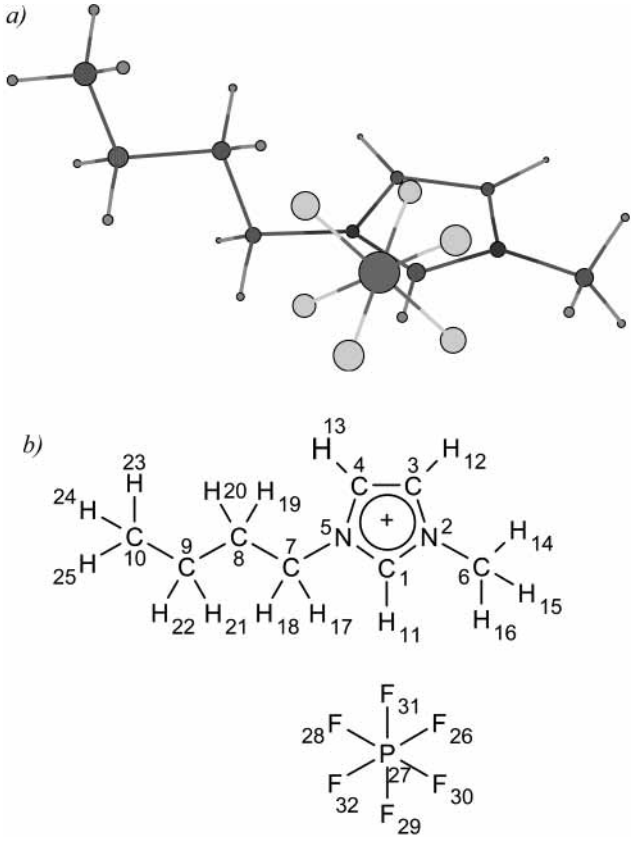

Figure 4. Ion pair $[C_4mim][PF_6]$: (a) overall view; (b) numbering of atoms.

S is the area of an effusion orifice. The significant scatter of the results and nearly exponential trend of ln *W* versus 1/*T* imply that the observations are experimental artifacts, not P_{sat}. The loss of mass in this experiment at $T > 473$ K was most likely caused by decomposition of the samples, which increased with temperature. When an uncovered liquid surface was used (experiment 10), *W* was much lower than in experiments with membranes. This indicates that when the evaporation surface area is large, Δm is determined by the rate of decomposition, not vaporization. Thus, one can speculate that liquid had begun to decompose at 473 K, coinciding with the sharp upward curvature in the DSC curve, shown in Figure 1. This finding is considerably lower than a reported decomposition temperature[2] of 622 K, given at the maximum slope of the TGA curve. At $T <$ 430 K when the sample was stable under vacuum conditions, the vapor pressure was too low to be determined accurately with our apparatus, but it clearly did not exceed 10^{-2} Pa.

Ideal Gas Thermodynamic Properties of [C₄mim][PF₆]. The procedure to calculate ideal gas thermodynamic properties has been described in detail.[3,4] The necessary molecular data for statistical calculations were obtained by quantum chemical calculations performed using the PC GAMESS version[5] of the GAMESS (US) QC package[6] and molecular mechanics calculations using the MM3 force field[7] in the TINKER package.[8] We conducted statistical mechanical calculations for a cation, an anion, and an ion pair of $[C_4mim][PF_6]$ in the ideal gas state and evaluated the dissociation constant for the ion pair.

The geometries of the cation, the anion, and the ion pair were optimized ab initio with the RHF/6-31G* basis set, as shown in Figure 4 and given in Table 2. The earlier calculations for the $[C_4mim]^+$ cation[9] agreed with this work. According to quantum chemical calculations by Meng et al.,[10] the ethyl top is in the gauche conformation, while our calculations show that the most stable conformation is the trans one. The HF/6-31G* total energies of the cation and the ion pair reported in ref 10 were approximately 0.002 Hartrees higher than those in Table 3. Bond lengths for the cation agree with those for $[C_{12}mim][PF_6]$ determined by X-ray diffraction[11] within 1%, and the difference for the anion did not exceed 1.5%. According to the calculations, in the most stable conformer, the anion is above the plane of the ring and is slightly displaced toward the butyl group, as shown in Figure 4. From the geometry and masses of the atoms, the principal moments of inertia for the cation, the anion, and the ion pair were calculated and are presented in Table 4. There are two chiral forms for the $[C_4mim][PF_6]$ ion pair. The plane of the imidazole ring is a chiral plane. The point group of the PF_6^- anion was O_h, and the overall symmetry number was 24.

Total energies for $[C_4mim]^+$, PF_6^-, and $[C_4mim][PF_6]$ were calculated with the MP2/6-31+G* basis set for the geometries obtained in the RHF/6-31G* calculations. The total energies of the cation, the anion, and the ion pair are given in Table 3. Energetic parameters of the minima and saddle points for the internal rotation of PF_6 and C_4H_9-tops were found in a similar way by using the MP2/6-31G* basis set for the RHF/6-31G* geometries.

An IR spectrum of liquid $[C_4mim][PF_6]$ in the range (400 to 3200) cm^{-1} was measured with a Perkin-Elmer FTIR Spectrometer 1000. The frequencies are given in Table 5. In general, the spectrum was in agreement with those reported previously.[12,13]

Assignment of frequencies (Table 5) was performed on the basis of the published data for PF_6^-,[14] for imidazole,[15,16] for 1-methylimidazole,[16] and for $[C_2mim][AlCl_4]$,[17] in ad-

Table 2. Spatial Coordinates of the $[C_4mim][PF_6]$ Ion Pair (Å = 10^{-10} m)

atom	*x*/Å	*y*/Å	*z*/Å	atom	*x*/Å	*y*/Å	*z*/Å
C_1	0.811	−1.661	−0.637	H_{17}	3.539	−0.034	−1.221
N_2	0.663	−2.850	−0.096	H_{18}	1.900	0.467	−1.597
C_3	1.867	−3.218	0.470	H_{19}	1.529	1.057	0.795
C_4	2.726	−2.216	0.246	H_{20}	3.196	0.658	1.154
N_5	2.044	−1.246	−0.460	H_{21}	2.277	2.819	−0.786
C_6	−0.593	−3.596	−0.034	H_{22}	3.948	2.436	−0.453
C_7	2.543	0.094	−0.815	H_{23}	3.224	4.416	0.863
C_8	2.529	1.040	0.383	H_{24}	3.607	3.097	1.953
C_9	2.951	2.455	−0.016	H_{25}	1.931	3.482	1.594
C_{10}	2.927	3.419	1.169	F_{26}	−2.034	−0.673	−0.818
H_{11}	0.039	−1.109	−1.122	P_{27}	−1.789	0.726	−0.017
H_{12}	1.994	−4.150	0.975	F_{28}	−0.498	0.976	−0.983
H_{13}	3.752	−2.101	0.518	F_{29}	−2.711	1.486	−1.055
H_{14}	−0.776	−3.886	0.990	F_{30}	−3.020	0.409	0.927
H_{15}	−0.531	−4.473	−0.663	F_{31}	−0.806	−0.090	0.985
H_{16}	−1.389	−2.949	−0.364	F_{32}	−1.462	2.070	0.760

Table 3. Total Energies and Zero-Point Vibrational Energies of the Species (1 au = 1 Hartree = 2625.5 kJ·mol⁻¹)

	E/au		ZPVE
	HF/6-31G*	MP2/6-31+G*// HF/6-31G*	kJ·mol⁻¹
$[C_4mim][PF_6]$	−1358.117 426	−1360.637 926	624.6
PF_6^-	−937.602 709	−938.762 625	50.2
$[C_4mim]^+$	−420.384 736	−421.734 411	571.0

Table 4. Principal Moments of Inertia of the Particles

	$I_A \times 10^{45}$	$I_B \times 10^{45}$	$I_C \times 10^{45}$	$I_A I_B I_C \times 10^{135}$
	kg·m²	kg·m²	kg·m²	kg·m²
$[C_4mim]^+$	2.066	16.284	16.885	568.08
$[PF_6]^-$	3.252	3.252	3.252	34.39
$[C_4mim][PF_6]$	19.010	23.225	37.347	16489.2

Table 5. Calculated[a] and Experimental Vibrational Wavenumbers for [C_4mim][PF_6]

HF/6-31G*						HF/6-31G*					
	intensity	IR					intensity	IR			
$\bar{\omega}_e$[a] / cm^{-1}	10^{-13} cd^2·kg^{-1}	$\bar{\omega}_e$ / cm^{-1}	transmn / %	form of vibration[b]	chosen $\bar{\omega}_e$ / cm^{-1}	$\bar{\omega}_e$[a] / cm^{-1}	10^{-13} cd^2·kg^{-1}	$\bar{\omega}_e$ / cm^{-1}	transmn / %	form of vibration[b]	chosen $\bar{\omega}_e$ / cm^{-1}
3164	17.9	3172	34	CH ring str	3172	983	0.19			CH ring o/p bend	989
3131	0.33			CH ring str	3126	972	0.44	975	94	Bu CC str	975
3113	0.89	3126	47	CH ring str	3126	921	0.20	950	86	CCH bend	950
3025	0.37	2967	36	CH_3(N) str	2967	886	0.61	880	14 sh	CH ring o/p bend	880
2994	1.08			CH_2 str	2967	881	5.83			Bu CC str	880
2985	1.90			CH_3(N) str	2967	885	68.7	838	3	PF str	838
2956	1.51	2940	44	CH_2 str	2940	895	72.5			PF str	838
2935	6.02			CH_3(C) str	2940	879	65.2			PF str	838
2923	9.98			CH_3(C) str	2940	777	0.06	780	58	CCH bend	780
2919	4.62			CH_2 str	2940	756	5.23	752	40	complex bend	752
2913	5.39	2878	50	CH_3(N) str	2878	710	4.76			PF str	735
2894	2.91			CH_2 str	2878	715	1.42	698	80	CCH bend	698
2868	6.13			CH_3(C) str	2878	705	3.03			complex bend	698
2861	2.72			CH_2 str	2878	648	7.44	651	58	ring o/p bend	651
2851	7.82			CH_2 str	2878	620	3.66	624	41	ring o/p bend	624
1589	4.38	1575	33	ring str	1575	605	0.26	600	80	ring o/p bend	600
1581	20.8			ring bend	1575	566	0.98			PF str	563
1485	0.88	1467	43	CH_2 bend	1466	559	2.46			PF str	563
1483	2.57			CH_3 bend	1466	528	10.8	558	11	FPF bend	558
1476	0.76			CH_2 bend	1466	525	5.38			FPF bend	558
1472	0.96			CH_3 bend	1466	524	6.05			FPF bend	558
1469	0.85			CH_3 bend	1466	444	0.22	471	83	FPF bend	470
1467	2.10			CH_3 bend	1466	440	0.03			FPF bend	470
1465	0.06			CH_2 bend	1466	437	0.00			FPF bend	470
1444	2.14	1431	60	ring str	1431	420	0.10	417		alkyl i/p bend	420
1439	2.51			CH_3(N) bend	1431	396	0.24			alkyl i/p bend	396
1407	1.51	1387	62	CH_3(C) bend	1387	311	0.14			alkyl o/p bend	312
1403	2.31			CCH bend	1387	297	0.01			FPF bend	320
1374	0.65			ring str	1387	295	0.00			FPF bend	320
1357	0.41	1340	67	CCH bend	1340	287	0.00			FPF bend	320
1318	2.16			CH ring bend	1340	275	0.20			complex bend	275
1312	0.06	1301	82	CCH bend	1301	239	0.11			alkyl o/p bend	239
1293	0.40			CCH bend	1301	236	0.01			Me(C) tors	
1277	1.16	1284	86	CCH bend	1284	202	0.21			complex bend	202
1276	0.63			CCH bend	1284	136	0.50			Et tors	
1213	1.11	1210	82 sh	CCH bend	1210	121	2.10			complex bend	121
1155	28.5	1170	19	ring str	1170	110	0.09			Me(N) tors	
1137	1.22	1114	64	Me CCH bend	1114	86	0.52			Pr tors	
1129	2.99			CC alkyl str	1114	80	0.96			Cat-An str	80
1103	0.65	1094	77	CCH bend	1094	60	0.42			Cat-An bend	60
1092	0.80			CH ring bend	1094	58	0.32			Bu tors	
1081	1.22			Me CCH bend	1094	55	0.18			Cat-An bend	55
1017	0.25	1028	78	CC str	1028	35	0.30			Cat-An bend	35
1008	1.23	1009	92 sh	ring i/p bend	1009	24	0.36			Cat-An bend	24
998	0.12	989	94	complex bend	989	21	0.18			Cat-An tors	

[a] The scaling factor 0.8953 was applied to the calculated values. [b] Note that i/p bend is in-plane bending; o/p bend is out-of-plane bending; alkyl bend is bending of alkyl groups relative to the ring; FPF bend is F−P−F valent angle bending in the anion. Cat-An vibrations are vibrations where the cation oscillates around the anion.

dition to calculations with the 6-31G* basis set. After a normal coordinate analysis was performed, the following wavenumbers (cm^{-1}) were selected to calculate the vibrational contributions of the ions to the thermodynamic properties in the ideal gas state (degeneracy is in parentheses). [PF_6]$^-$: 320(3), 462(3), 558(3), 563(2), 735, 838(3). [C_4mim]$^+$: [32, 69], 73, [87, 110], 191, [230], 237, 262, 303, 387, 420, 600, 624, 651, 698(2), 771, 780, 880, 905, 909, 950, 975, 989, 1009, 1028, 1094(3), 1114(2), 1170, 1210, 1284(2), 1301(2), 1340(2), 1387(3), 1431(2), 1466(7), 1575-(2), 2878(5), 2940(4), 2967(3), 3126(3). Zero-point vibrational energies for the cation, the anion, and the ion pair (Table 3) were evaluated from the above data.

The wavenumbers (21, 58, 86, 110, 136, and 236) cm^{-1} assigned to the rotation of the tops PF_6, C_4H_9−, C_3H_7−, CH_3−(N), C_2H_5−, and CH_3−(C), respectively, were not used in evaluating the vibrational contributions to the thermodynamic functions in the ideal gas state. The contribution of rotation for these tops was calculated separately, as described below. In a similar way, the wavenumbers (32, 69, 87, 110, and 230) cm^{-1} assigned to rotation of the groups C_4H_9−, C_3H_7−, CH_3−(N), C_2H_5−, and CH_3−(C) in the cation were excluded.

Parameters of Internal Rotation. The contributions of the six frequencies for the ion pair and the five frequencies for the cation were substituted with the contributions of internal rotation for the corresponding tops. The reduced moments of inertia of the tops calculated according to Pitzer[18] are given in Tables 6 and 7. Rotation of the CH_3−(N) top was assumed to be unrestricted, with the symmetry number $\sigma_r = 3$. This assumption was based on the fact that barriers to internal rotation for methyl tops attached to aromatic rings are close to zero. The rotational contribution of this top to the thermodynamic functions was evaluated by use of a classical approximation.

Energy differences between conformers and barriers to internal rotation for the butyl top in the cation and the ion pair were calculated as described above. There were

Table 6. Parameters of Internal Rotation in [C₄mim][PF₆]

top	$I_r \times 10^{47}$ / kg·m²	σ_r	V_0 / J·mol⁻¹	V_1 / J·mol⁻¹	V_2 / J·mol⁻¹	V_3 / J·mol⁻¹
PF_6	271.1	3	3940	0	0	3940
CH_3−(N)	5.21	3	0	0	0	0
C_4H_9−	217.1	1	10110	3960	−6150	0
C_3H_7−	87.70	1	9500	3770	1100	6840
C_2H_5−	53.26	1	9310	3490	1010	6830
CH_3−(C)	5.15	3	5640	0	0	5640

Table 7. Parameters of Internal Rotation in [C₄mim]⁺

top	$I_r \times 10^{47}$ / kg·m²	σ_r	V_0 / J·mol⁻¹	V_1 / J·mol⁻¹	V_2 / J·mol⁻¹	V_3 / J·mol⁻¹
CH_3−(N)	5.12	3	0	0	0	0
C_4H_9−	61.65	1	2500	1465	2390	0
C_3H_7−	47.29	1	9500	3770	1100	6840
C_2H_5−	33.90	1	9310	3490	1010	6830
CH_3−(C)	5.08	3	5640	0	0	5640

two minima on potential curves for both the ion pair and the cation, as would be expected. The saddle points in the pair were of different amplitudes (16.1 and 17.1) kJ·mol⁻¹. Since the difference was not large, the potential energy curve could be approximated by the function

$$V(\varphi) = \sum_{i=0}^{n} V_i \cos(n\varphi) \qquad (2)$$

where n is the number of maxima. The PF_6^- top was assumed to rotate about the line defined by the P_{27} and C_1 atoms and had a 3-fold barrier. The barrier calculated with the MP2/6-31G* basis set was 7.9 kJ·mol⁻¹. The energetic parameters of the internal rotation for the CH_3−, C_2H_5−, and C_3H_7− tops of the butyl group were assumed to be equal to those in hexane and were found by molecular mechanics using the MM3(99) force field.[7] Potential energy curves for the rotation of the tops were approximated by functional forms represented by eq 2. Their parameters were determined by a least-squares method and are presented in Tables 6 and 7. The contributions of all the tops except CH_3−(N) were evaluated by the energy levels obtained solving the Schrödinger equation with the potential energy given in eq 2.

Thermodynamic functions of the cation, anion, and ion pair are given in Tables 8 to 10. From the data in Tables 3 and 8−10, one can conclude that in the ideal gas the substance exists mainly in the form of ion pairs ($K_{dis} = 7 \times 10^{-31}$ at 500 K). Thus, the properties of the ion pair are the properties of the substance in the ideal gas state.

Monte Carlo simulations[9] have estimated the cohesive energy density c of liquid [C_4mim][PF_6] to be 712 J·cm⁻³ over the range of temperatures from (298 to 343) K and of pressures from (0.98 to 2028) bar and estimated the molar volume of the liquid V_L to be 200.8 cm³·mol⁻¹ at 298 K. From these values, we calculated the change of internal energy at vaporization

$$\Delta_{vap}U^\circ = cV_L$$

where V_L is the molar volume of the liquid and $\Delta_{vap}U^\circ$ = 142.8 kJ·mol⁻¹. On the basis of a comparison of the calculated molar volume[9] of [C_4mim][PF_6] at 298 K (200.8 cm³·mol⁻¹) and the measured volume from our pycnometer[19] (207.9 cm³·mol⁻¹), we estimate the uncertainty of the calculated molar volume value to be 3.5%. Since the cited value of c was not characterized with an uncertainty in ref 9, we estimated the uncertainty of the calculated value of $\Delta_{vap}U^\circ$ to be twice the uncertainty of V_L. This $\Delta_{vap}U^\circ$ value was used to obtain the enthalpy of vaporization

$$\Delta_{vap}H^\circ = \Delta_{vap}U^\circ + RT = 145 \text{ kJ·mol}^{-1}$$

The uncertainty of $\Delta_{vap}H^\circ$ was assumed to be 7% to be consistent with the estimated uncertainty of $\Delta_{vap}U^\circ$. Furthermore, we calculated the value of $\Delta^g_{liq}C_p = C_p(g) - C_p(l) = (95 \pm 3)$ J·K⁻¹·mol⁻¹ from unpublished heat capacity data[19] of liquid [C_4mim][PF_6] determined in our laboratory with a DSC and the heat capacity in the ideal gas state reported in this work. We found this value to be constant, within the estimated uncertainties, in the range of temperatures from (298.15 K to 500) K. From the calculated value of $\Delta^g_{liq}C_p$, we then calculated the temperature dependence of the enthalpy of vaporization, given in Table 11. The entropy of vaporization given in Table 11 was estimated in the following way: $S°_{298}$(g) was evaluated from statistical calculations discussed earlier and reported in Table 8; $S°_{298}$(l) was estimated from our unpublished

Table 8. Thermodynamic Properties of [C₄mim][PF₆] (M = 284.182 36 g·mol⁻¹) in the Ideal Gas State[a]

T / K	$S°$ / J·K⁻¹·mol⁻¹	C_p / J·K⁻¹·mol⁻¹	$(H°(T) - H°(0))/T$ / J·K⁻¹·mol⁻¹	$-(G°(T) - H°(0))/T$ / J·K⁻¹·mol⁻¹
50	340.0	107.2	75.47	264.5
100	427.3	150.9	102.0	325.3
150	497.1	195.6	125.9	371.2
200	559.1	237.3	148.6	410.6
298.15	668.4	313.8	190.6	477.8
300	670.3	315.1	191.3	479.0
400	770.6	383.0	231.0	539.5
500	862.2	438.1	267.1	595.0
600	946.1	482.1	299.4	646.7
700	1023.2	517.9	328.2	695.0
800	1094.3	547.6	353.8	740.5
900	1160.3	572.5	376.7	783.6
1000	1221.7	593.7	397.4	824.3
1100	1279.2	611.7	416.1	863.1
1200	1333.1	627.1	433.0	900.0
1300	1383.8	640.4	448.5	935.3
1400	1431.7	651.8	462.6	969.1
1500	1477.0	661.7	475.6	1001.5

[a] R = 8.314 472 J·K⁻¹·mol⁻¹; $p°$ = 10⁵ Pa.

Table 9. Thermodynamic Properties of [C₄mim]⁺ (M = 139.218 18 g·mol⁻¹) in the Ideal Gas State[a]

T / K	$S°$ / J·K⁻¹·mol⁻¹	C_p / J·K⁻¹·mol⁻¹	$(H°(T) - H°(0))/T$ / J·K⁻¹·mol⁻¹	$-(G°(T) - H°(0))/T$ / J·K⁻¹·mol⁻¹
50	271.3	65.60	50.23	221.1
100	326.3	96.82	65.70	260.6
150	370.6	121.7	80.45	290.1
200	408.3	141.9	93.30	315.0
298.15	473.0	186.3	116.4	356.6
300	474.1	187.2	116.8	357.3
400	534.8	237.0	140.6	394.2
500	592.7	282.8	164.6	428.1
600	647.8	322.0	187.6	460.2
700	700.0	355.2	209.3	490.8
800	749.4	383.4	229.3	520.0
900	795.9	407.4	247.8	548.1
1000	840.0	428.1	264.8	575.1
1100	881.6	445.8	280.5	601.1
1200	921.1	461.1	294.9	626.2
1300	958.5	474.3	308.2	650.3
1400	994.1	485.7	320.5	673.6
1500	1028.0	495.6	331.9	696.1

[a] R = 8.314 472 J·K⁻¹·mol⁻¹; $p°$ = 10⁵ Pa.

Table 10. Thermodynamic Properties of $[PF_6]^-$ (M = 144.964 18 g·mol^{-1}) in the Ideal Gas State[a]

T	$S°$	C_p	$(H°(T) - H°(0))/T$	$-(G°(T) - H°(0))/T$
K	J·K^{-1}·mol^{-1}	J·K^{-1}·mol^{-1}	J·K^{-1}·mol^{-1}	J·K^{-1}·mol^{-1}
50	199.5	33.48	33.28	166.2
100	224.3	40.99	34.75	189.5
150	243.9	57.74	39.48	204.4
200	263.1	76.10	46.36	216.7
298.15	299.1	104.5	61.17	238.0
300	299.8	104.9	61.43	238.4
400	332.6	122.6	74.71	257.9
500	361.2	133.2	85.43	275.8
600	386.1	139.9	93.99	292.1
700	408.0	144.2	100.9	307.2
800	427.5	147.2	106.5	321.0
900	445.0	149.4	111.2	333.8
1000	460.8	150.9	115.1	345.8
1100	475.2	152.1	118.4	356.9
1200	488.5	153.0	121.2	367.3
1300	500.8	153.7	123.7	377.1
1400	512.2	154.3	125.9	386.4
1500	522.9	154.8	127.8	395.1

[a] R = 8.314 472 J·K^{-1}·mol^{-1}; $p°$ = 10^5 Pa.

Table 11. Evaluated Saturated Vapor Pressures for $[C_4mim][PF_6]$ ($\delta\Delta_{vap}S° \approx$ 20 J·K^{-1}·mol^{-1}; $\delta[\ln\{P_{sat}(T)/P°\}] \approx$ 3.4 to 4.7)

T/K	$\Delta_{vap}H°$/kJ·mol^{-1}	$\Delta_{vap}S°$/J·K^{-1}·mol^{-1}	P_{sat}/Pa
298.15	145 ± 10	200	1×10^{-10}
400	135 ± 9.5	170	2×10^{-4}
500	126 ± 8.8	150	5×10^{-1}

calorimetric measurements in an adiabatic calorimeter in the range (100 to 320) K and in a differential scanning calorimeter[16] in the range (300 to 500) K; the ($S°_{100}$(cr) − $S°_0$(cr)) value was found from extrapolation, by applying the method of Kelley, Parks, and Huffman,[20] to within an estimated uncertainty of 10% (±14 J·K^{-1}·mol^{-1}). The overall uncertainty of $\Delta_{vap}S°$ is estimated to be ±20 J·K^{-1}·mol^{-1}.

Vapor pressures of $[C_4mim][PF_6]$, presented in Table 11, were estimated by applying the thermodynamic relation

$$-RT \ln\{P_{sat}(T)/P°\} = \Delta_{vap}H°(T) - T\Delta_{vap}S°(T)$$

Since the vapor pressures' uncertainties are much greater than the values themselves, the results given in Table 11 should be interpreted as order-of-magnitude estimates only. The calculated vapor pressure at 298.15 K is 10^{-10} Pa. Though this value is considerably smaller than the experimental range of the Knudsen effusion technique, approximate measurements would be feasible by using a gas saturation method that employs very long times for elution. Soon, we plan to revise the estimated ($S°_{100}$(cr) − $S°_0$(cr)) value from direct measurements of saturated liquid heat capacity C_{sat} by adiabatic calorimetry in the liquid helium temperature range.

Literature Cited

(1) Krasulin, A. P.; Kozyro, A. A.; Kabo, G. J. Saturated vapor pressure of urea in the temperature range 329−403 K. *Zh. Prikl. Khim.* **1987**, *60* (1), 104−108.

(2) Huddleston, J. G.; Visser, A. E.; Reichert, W. M.; Willauer, H. D.; Broker, G. A.; Rogers, R. D. Characterization and comparison of hydrophilic and hydrophobic room-temperature ionic liquids incorporating the imidazolium cation. *Green Chem.* **2001**, *3*, 156−164.

(3) Frenkel, M. L.; Kabo, G. J.; Marsh, K. N.; Roganov, G. N.; Wilhoit, R. C. *Thermodynamics of organic compounds in the gas state*; TRC: College Station, TX, 1994; Vol. I.

(4) Stull, D. R.; Westrum, E. F., Jr.; Sinke, G. C. *The Chemical Thermodynamics of organic compounds*; John Wiley & Sons: 1969.

(5) Granovsky, A. A. http://classic.chem.msu.su/gran/gamess/index.html.

(6) Schmidt, M. W.; Baldridge, K. K.; Boatz, J. A.; Elbert, S. T.; Gordon, M. S.; Jensen, J. J.; Koseki, S.; Matsunaga, N.; Nguyen, K. A.; Su, S.; Windus, T. L.; Dupuis, M.; Montgomery, J. A. General atomic and molecular electronic structure system. *J. Comput. Chem.* **1993**, *14*, 1347−1363.

(7) Allinger, N. L.; Yuh, Y. H.; Li, J.-H. Molecular Mechanics. The MM3 Force Field for Hydrocarbons. 1. *J. Am. Chem. Soc.* **1989**, *111*, 8551−8566.

(8) Pappu, R. V.; Hart, R. K.; Ponder, J. W. Analysis and application of potential energy smoothing and search methods for global optimization. *J. Phys. Chem. B* **1998**, *102*, 9725−9742.

(9) Shah, J. K.; Brennecke, J. F.; Maginn, E. J. Thermodynamic properties of the ionic liquid 1-*n*-butyl-3-methylimidazolium hexafluorophosphate from Monte Carlo simulations. *Green Chem.* **2002**, *4* (2), 112−118.

(10) Meng, Z.; Dölle, A.; Carper, W. R. Gas-phase model of an ionic liquid: semiempirical and ab initio bonding and molecular structure. *J. Mol. Struct. (THEOCHEM).* **2002**, *585*, 119−128.

(11) Gordon, C. M.; Holbrey, J. D.; Kennedy, A. R.; Seddon, K. R. Ionic liquid crystals: hexafluorophosphate salts. *J. Mater. Chem.* **1998**, *8*, 2627−2636.

(12) Koel, M. Physical and chemical properties of ionic liquids based on the dialkylimidazolium cation. *Proc. Estonian Acad. Sci. Chem.* **2000**, *49*, 145−155.

(13) Suarez, P. A. Z.; Einloft, S.; Dullius, J. E. L.; de Souza, R. F.; Dupont, J. Synthesis and physical-chemical properties of ionic liquids based on 1-*n*-butyl-3-methylimidazolium cation. *J. Chim. Phys.* **1998**, *95*, 1626−1639.

(14) Buhler, K.; Bues, W. Schwingungsspektren von Fluorophosphatschmelzen und -kristallen. *Z. Anorg. Allg. Chem.* **1961**, *308*, 62−69.

(15) Cordes de N. D., M.; Walter, J. L., C. S. C. Infrared and Raman spectra of heterocyclic compounds − I. The infrared studies and normal vibrations of imidazole. *Spectrochim. Acta* **1968**, *24A*, 237−252.

(16) http://www.aist.go.jp/RIODB/SDBS/11.05.02.

(17) Tait, S.; Osteryoung, R. A. Infrared study of ambient-temperature chloroaluminates as a function of melt acidity. *Inorg. Chem.* **1984**, *23*, 4352−4360.

(18) Pitzer, K. S. Energy levels and thermodynamic functions for molecules with internal rotation. *J. Chem. Phys.* **1946**, *14*, 239.

(19) Kabo, G. J., Belarusian State University, Minsk, Belarus, personal communication.

(20) Kelley, K. K.; Parks, G. S.; Huffman, H. M. A new method for extrapolating specific heat curves of organic compounds below the temperature of liquid air. *J. Phys. Chem.* **1929**, *33*, 1802.

Received for review July 25, 2002. Accepted September 22, 2002.

JE025591I